

RESEARCH ARTICLE

10.1002/2017JD027719

Key Points:

- Aerosol optical depth over India is calculated and compared with observations (satellite and AERONET)
- Model reproduces the observed fine mode aerosols; the composition of the aerosols shows importance of black carbon and dust over India
- The Indo-Gangetic Plain is the most polluted region over India, and this region control aerosols over Eastern India

Supporting Information:

- Supporting Information S1

Correspondence to:

A. R. Ravishankara,
a.r.ravishankara@colostate.edu

Citation:

David, L. M., Ravishankara, A. R., Kodros, J. K., Venkataraman, C., Sadavarte, P., Pierce, J. R., et al. (2018). Aerosol optical depth over India. *Journal of Geophysical Research: Atmospheres*, 123, 3688–3703. <https://doi.org/10.1002/2017JD027719>

Received 10 SEP 2017

Accepted 31 JAN 2018

Accepted article online 6 FEB 2018

Published online 13 APR 2018

Aerosol Optical Depth Over India

Liji Mary David¹ , A. R. Ravishankara¹ , John K. Kodros² , Chandra Venkataraman³, Pankaj Sadavarte^{3,4}, Jeffrey R. Pierce² , Sreelekha Chaliyakunnel⁵ , and Dylan B. Millet⁵ 

¹Department of Chemistry and Department of Atmospheric Science, Colorado State University, Fort Collins, CO, USA, ²Department of Atmospheric Science, Colorado State University, Fort Collins, CO, USA, ³Department of Chemical Engineering, Indian Institute of Technology Bombay, Mumbai, India, ⁴Institute for Advanced Sustainability Studies, Potsdam, Germany, ⁵Department of Soil, Water, and Climate, University of Minnesota, Twin Cities, St. Paul, MN, USA

Abstract Tropospheric aerosol optical depth (AOD) over India was simulated by Goddard Earth Observing System (GEOS)-Chem, a global 3-D chemical-transport model, using SMOG (Speciated Multi-pollutant Generator from Indian Institute of Technology Bombay) and GEOS-Chem (GC) (current inventories used in the GEOS-Chem model) inventories for 2012. The simulated AODs were ~80% (SMOG) and 60% (GC) of those measured by the satellites (Moderate Resolution Imaging Spectroradiometer and Multi-angle Imaging SpectroRadiometer). There is no strong seasonal variation in AOD over India. The peak AOD values are observed/simulated during summer. The simulated AOD using SMOG inventory has particulate black and organic carbon AOD higher by a factor ~5 and 3, respectively, compared to GC inventory. The model underpredicted coarse-mode AOD but agreed for fine-mode AOD with Aerosol Robotic Network data. It captured dust only over Western India, which is a desert, and not elsewhere, probably due to inaccurate dust transport and/or noninclusion of other dust sources. The calculated AOD, after dust correction, showed the general features in its observed spatial variation. Highest AOD values were observed over the Indo-Gangetic Plain followed by Central and Southern India with lowest values in Northern India. Transport of aerosols from Indo-Gangetic Plain and Central India into Eastern India, where emissions are low, is significant. The major contributors to total AOD over India are inorganic aerosol (41–64%), organic carbon (14–26%), and dust (7–32%). AOD over most regions of India is a factor of 5 or higher than over the United States.

Plain Language Summary Overhead amounts of particulate matter, their chemical make up, and their variations over India, a highly polluted and fast developing country, were calculated using a global model. It shows that the particulate pollution levels over the Indo-Gangetic Plain is more than 5 times higher than over the United States. The use of the most recent available emission inventory shows that there is more black carbon, from incomplete combustion, than estimated using the existing regional inventory. The calculations also show that the cleanest part is the very Northern India and that pollution over Eastern India is significantly influenced by what happens over the Indo-Gangetic Plain.

1. Introduction

Aerosols in the troposphere can affect Earth's climate by scattering and absorbing the incoming solar radiation directly as well as by altering cloud amounts and properties (Boucher et al., 2013). Aerosols, often called particulate matter (PM), are one of the major constituents of air pollution, especially in the developing world. Furthermore, they also alter visibility and provide a substrate for heterogeneous and multiphase reactions. Aerosols have a wide range of sizes, composition, optical properties, chemical properties, and abilities to alter clouds.

Both natural processes and anthropogenic activities are responsible for aerosols in the troposphere. While fine-mode (FM) aerosols (defined here as $PM_{2.5}$, PM that are 2.5 μm or less in diameter) in the atmosphere come mainly from gas-to-particle conversion (from anthropogenic and biogenic emissions), coarse-mode (CM) aerosols arise mostly from natural sources (such as from deserts, oceans, volcanoes, and biosphere), with possible contributions from some human activities. The natural global aerosol mass is dominated by dust, sea salt, and sulfate produced over the ocean surface (Prospero et al., 2002). Anthropogenic activities have caused considerable changes in aerosol composition and loading, particularly over South Asia. A significant fraction of aerosols over India are absorbing (black carbon (BC)), and hence, they are expected to lead to

warming and influence the water cycle in this region (e.g., Indian summer monsoon) (Lau et al., 2006; Ramanathan et al., 2005). Over India, dust may not be confined only to desert (Philip et al., 2017).

India is projected to be the most populous country in the world in the coming decades with more than a sixth of the world's population. There are rapid expansions of urbanization, manufacturing, agricultural activities, and energy utilization, which have led to an increase in anthropogenic emissions and deterioration of air quality. India is home to 33 of the 100 and 22 out of the top 50 most polluted cities in the world (World Health Organization, 2016), and New Delhi is often considered the most polluted city in the world. Pollution is not confined to urban areas; it is also common in rural areas where burning of wood, dung, and biomass for cooking and heating drive up pollution levels.

The Indo-Gangetic Plain (IGP) has persistent high aerosol optical depth (AOD) as observed by ground-based (e.g., Aerosol Robotic Network (AERONET)) and satellite-based (e.g., Moderate Resolution Imaging Spectroradiometer (MODIS), Multi-angle Imaging SpectroRadiometer (MISR)) measurements (e.g., Prasad & Singh, 2007; Ramachandran & Kedia, 2013). About 80% of the 158 cities in the country exceed the Indian National Ambient Air Quality Standard for PM_{10} of $60 \mu\text{g}/\text{m}^3$, 40 cities are designated as "high-pollution" areas with annual mean PM_{10} levels of $61\text{--}90 \mu\text{g}/\text{m}^3$, and 85 are designated as "critical" ($>90 \mu\text{g}/\text{m}^3$), exceeding the PM_{10} standard by over 1.5 times (Central Pollution Control Board, 2014). Anthropogenic aerosol emissions, in contrast to the decreasing emission trends over Europe and North America, are increasing in South Asia in recent decades (Babu et al., 2013; de Meij et al., 2012; Granier et al., 2011; Ohara et al., 2007).

Aerosol properties can be derived from ground-based (limited spatial but high temporal coverage) and satellite (large spatial coverage but less frequent) observations. However, satellite-derived AOD requires inversion procedures and they exhibit larger uncertainties compared to ground-based retrievals. The uncertainties in satellite derived AOD are higher over land where surface reflectance cannot be neglected and where several assumptions are required pertaining to aerosol type and underlying surface features (Kaufman et al., 1997; Levy et al., 2013). Satellite-derived values are often assessed relative to ground-based observations (Kahn et al., 2010; Levy et al., 2010). Therefore, chemical-transport models, themselves evaluated against ground and satellite observations, can provide higher spatial and temporal scale information on pollutant emissions, air quality, aerosol radiative forcing, visibility, and global climate change. Meanwhile, uncertainties in chemical-transport models arise from uncertainties in meteorological fields, emission inventories, boundary conditions, and representation of chemical processes and deposition. Chemical-transport models have been used to study AOD globally and over specific regions such as Asia, the United States, and Europe (e.g., Li et al., 2013, 2016; Misra et al., 2016). Studies of AOD using global models have shown that aerosol loading is underestimated in models over the IGP in winter (Chin et al., 2009; Henriksson et al., 2011; Sanap et al., 2014). Satellite-derived AOD has been extensively checked against ground-based observations over the Indian region (e.g., Jethva et al., 2007; Tripathi et al., 2005).

Clearly, a comprehensive model-based inquiry into aerosols over India is lacking, especially when one wants to examine how aerosols vary from region to region, evaluate the role of transport from one region to another (an essential examination for any policy actions), and how the calculated aerosols vary with emissions. The latter point is especially important since the emission inventories over India are not as extensive as those for the developed world. Lastly, systematic observations of aerosols from ground-based instruments are lacking (or not widely reported), and hence, one has to employ models to obtain a comprehensive picture of aerosols over India. These are the factors that motivated our study.

In this study, we use Goddard Earth Observing System (GEOS)-Chem (GC), a chemical-transport model, to examine aerosols over the Indian region. AOD was simulated using two different emission inventories, and the calculated AOD was compared with observations from satellites and ground-based measurements. We also characterize (i) model deficiency in reproducing the observations, and provide recommendations for future improvement, and (ii) the aerosol composition over different regions in India. The outcome of this study emphasizes the need for measurements of aerosol composition over various regions of India to understand their sources, which are necessary first steps to develop any mitigation strategy. Our work also highlights the role of dust over India.

A description of the study region, meteorology, and division of India into distinct regions is given in section 2 followed by a description of our model and observational data from satellites and ground-based

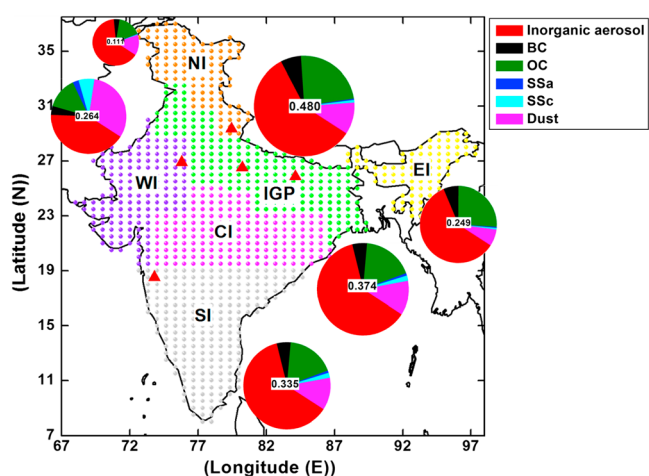


Figure 1. A map of India divided into six regions based on meteorology and variation of aerosols. Spatial distribution of GEOS-Chem grid points ($0.5^\circ \times 0.667^\circ$ resolution) over the Indian region is shown in different colors for the different regions. Five Aerosol Robotic Network sites that provided aerosol optical depth (AOD) data for 2012 are shown as red triangles. Satellite data were regridded to the GEOS-Chem grid points. Distribution of AOD at 550 nm and composition of aerosols across the six regions over India simulated by the model (using SMOG emission inventory) are shown in the pie chart. The number in each pie represents the calculated AOD averaged over the region. The percentage of aerosol component in the pie chart for each region is given in Table 2.

measurements in section 3. In section 4, AOD simulations using emission estimates from SMOG (Speciated Multi-pollutant Generator developed by Indian Institute of Technology (IIT) Bombay) (Pandey et al., 2014; Sadavarte & Venkataraman, 2014) and current emission inventories in the model (denoted here as GC) are compared with observations from satellite and ground stations. We provide monthly and regional statistics of observed versus calculated FM and CM AOD. We also discuss possible causes for the model underestimation of AOD based on employed emission inventories in this section. Major findings from this study are summarized in section 5.

2. Study Region

India (7.5° – 37.5° N and 68° – 99° E) has large heterogeneities in topography, aerosol properties, and meteorology. It comprises the Himalayas in the north, the IGP that extends from the foothills of Himalayas to the southern central plateau, the Thar Desert in the northwest, and the southern peninsula separated from the coastal regions by the Eastern and Western Ghats. The IGP has the highest population density in India and is characterized by large aerosol precursor emission sources.

Overall, there is a large aerosol burden over India due to (i) large sources of local dust that tends to be lofted under hot and dry conditions, (ii) smoke from agricultural burning, (iii) anthropogenic pollution, and (iv) long-range transport from deserts in Asia and Africa (Dey et al., 2004; Giles et al., 2011; Misra et al., 2014; Sharma et al., 2010; Sijikumar et al., 2016). However, the major source of FM aerosols ($PM_{2.5}$) is still likely to

be secondary aerosols formed from emissions such as SO_2 with contributions from BC and organic carbon (OC) over India (Henriksson et al., 2011).

India experiences a tropical and subtropical climate, which is strongly influenced by the Himalayas, the Thar Desert, and oceans that surround the peninsular part of the country. The northern region of the country has a continental climate with severe summers and cold to mild winters. The coastal regions are warm with frequent rains throughout the year. The subcontinent experiences strong reversal of winds twice in a year in the lower troposphere. Based on this meteorology, India's seasons are best classified as winter (December/January–February), premonsoon/summer (March–May), monsoon (June–August/September), and postmonsoon (October–November). Further information about this classification is given in supporting information (section S1).

IGP has a tendency to retain pollution within the region during winter, being somewhat removed from marine influences (Kar et al., 2010). In contrast, marine air masses prevail over much of southern India, surrounded in the east, west, and south by oceans; hence, cleaner air is generally expected over this region compared to IGP. While Eastern India (EI) is likely to be highly influenced by what happens over IGP, Northern India (NI) is unlikely to be influenced by the emissions from the rest of India. Based on the meteorological considerations and influences noted above, we have divided India into six regions (NI, IGP, EI, Western India (WI), Central India (CI), and Southern India (SI)) as shown in Figure 1. The figure also shows the location of ground-based AERONET stations (shown in red triangles), whose data are used in this paper for comparisons with satellite data and simulated AOD. It is important to note the above regional separations based on geography and meteorology rather than population and economic output.

3. Description of Model and Observations

3.1. GEOS-Chem AOD Simulation

In this study, we used the GEOS-Chem global 3-D model (version 10-01) driven by meteorological data assimilated by the GEOS at the NASA Global Modeling and Assimilation Office (Bey et al., 2001). The model has fully coupled tropospheric NO_x - O_x -hydrocarbon-aerosol chemistry. The GEOS-Chem emissions were configured

using the Harvard-NASA Emissions Component module. The present study used GEOS-5 meteorology, with a temporal resolution of 6 h (3-D fields such as u and v wind components and temperature) and 3 h for surface variables and mixing depths (such as soil moisture, heat fluxes, and albedo). The horizontal resolution was $0.5^\circ \times 0.667^\circ$ with 47 eta vertical levels from the surface to ~ 80 km. For the global $2^\circ \times 2.5^\circ$ GEOS-Chem model runs, the horizontal resolution of the meteorological fields was altered to match the model grid. In the nested grid GEOS-Chem model, the native high horizontal resolution over the nested regional domain was retained.

In addition to the global simulations, GEOS-Chem nested simulations were carried out at GEOS-5 horizontal resolution for the Indian region ($\sim 0^\circ$ – 41° N latitude, $\sim 56^\circ$ – 107° E longitude) to determine AOD at 400/440 nm, 500/550 nm, and 1,020 nm wavelengths. To produce the nested simulation, global simulations were run first to generate the initial boundary conditions for all species. Thereafter, the higher-resolution meteorological data were used to calculate AODs within the nested grid. We ran GEOS-Chem v10-01 at $0.5^\circ \times 0.667^\circ$ horizontal resolution and 47 vertical levels for 2012. Figure 1 shows the GEOS-Chem $0.5^\circ \times 0.667^\circ$ grid (959 grid points) over India.

The optical depth in each layer in the troposphere (from the surface up to ~ 18 km) was integrated to yield the column AOD as given by the following equation:

$$\tau = \sum_{\text{layer}=1}^{38} (\text{OPSNA} + \text{OPBC} + \text{OPOC} + \text{OPSSa} + \text{OPSSc} + \text{OPD})$$

where OPSNA represents the cumulative inorganic AOD and includes sulfate, nitrate, ammonium, and other water-soluble aerosols. OPBC, OPOC, OPSSa, and OPSSc, respectively, are the optical depths for BC, OC, accumulation sea salt, and CM sea-salt aerosols. OPD is the optical depth for dust in seven bins with the effective radii of dust particles ranging from $0.15 \mu\text{m}$ to $4.0 \mu\text{m}$. The contribution of stratospheric aerosol was very small in 2012, a time not influenced by major volcanic eruptions. The aerosol optical properties used by GEOS-Chem are based on the Global Aerosol Data Set (Koepke et al., 1997) with updates based on new observations (e.g., Drury et al., 2010). The data from Global Aerosol Data Set consist of wavelength-resolved complex refractive indices and estimates of the aerosol size distributions (geometric mean and standard deviation) at eight different relative humidity values (0, 50, 70, 80, 90, 95, and 99%). These were supplied to a Mie code (Mishchenko et al., 1999), which generated the optical properties assuming a log-normal distribution. The output includes extinction efficiency (Q_{ext}) and effective radius (r_{eff}), which are required for AOD calculations. The process is described in detail in Martin et al. (2003). The AOD was calculated using the following equation:

$$\tau = \frac{3 Q_{\text{ext}} M}{4 r_{\text{eff}} \rho}$$

where M is the column mass loading and ρ is the particle mass density (Tegen & Lacis, 1996). The global anthropogenic emissions of SO_2 , CO, NO_x , volatile organic compounds (VOCs), and NH_3 were from the regional MIX (a mosaic Asian anthropogenic emission inventory) emission inventory for Asia (Li et al., 2017). The OC and BC emissions were from Bond et al. (2007). The biomass burning emissions were from the Global Fire Emissions Database version 4 (Giglio et al., 2013). The biogenic VOC emissions were from the Model of Emissions of Gases and Aerosols from Nature version 2.1 inventory of Guenther et al. (2012) as implemented in GEOS-Chem by Hu et al. (2015). Emissions from other natural sources (e.g., lightning and volcanoes) were also included (Fisher et al., 2011; Murray et al., 2012). The mineral dust simulation in the model follows the Dust Entrainment and Deposition scheme of Zender et al. (2003) combined with a topographic source function (Chin et al., 2004; Ginoux et al., 2001), and sea-salt emissions employ the algorithm of Jaeglé et al. (2011). Therefore, dust and sea-salt fluxes in the model are independent of the anthropogenic, biogenic, and pyrogenic emission inventories used for other species. We have also simulated AOD using SO_2 , OC, and BC emissions from SMOG for 2013 provided by IIT Bombay (Pandey et al., 2014; Sadavarte & Venkataraman, 2014) (<https://sites.google.com/view/smogindia>). The SMOG emission inventory is for 2013. Unfortunately, the GEOS-5 meteorological fields are available for only up to June 2013. Therefore, we have used the 2013 emissions with 2012 meteorology, with the assumption that the emissions did not change significantly between 2012 and 2013.

3.2. Observations

We used satellite and ground-based observations for 2012 to compare with our calculated values. These included AERONET data from the five stations shown in Figure 1 and MODIS and MISR satellite observations.

Satellite observations. For this study, we used AOD measurements from two MODIS instruments aboard the Aqua and Terra satellites. Aqua and Terra satellites cross the equator, respectively, at ~1:30 p.m. and ~10:30 a.m. (local time). We used the Level 2 (L2 collection 6) MODIS aerosol product. We have used the “Optical depth land and ocean” product, which gives AOD over land with the highest quality (quality flag = 3) at 550 nm. The MODIS L2 provides full global coverage of aerosol properties using the Dark Target (over ocean) and Deep Blue (over land) algorithms. In collection 6, the Deep Blue algorithm covers the entire land area including both dark and bright surfaces. It has a spatial resolution of 10 km at nadir. For our analysis both Aqua and Terra AOD data were regridded to the model resolution.

The MISR instrument (aboard the Terra satellite) crosses the equator at ~10:30 a.m. (local time). MISR retrieves particle size and single scattering albedo. The narrow swath of MISR limits global coverage to every 9 days at the equator. We have used the Level 2 (version 22) aerosol data with a spatial resolution of 17.6 km downloaded from the NASA Langley Research Center Atmospheric Sciences Data Center (<http://eosweb.larc.nasa.gov>). Total column AOD is reported in the MISR product “RegBestEstimateSpectralOptDepth” that represents the mean AOD of all the mixtures that pass goodness of fit tests. The fractional contribution of each aerosol component was calculated using the method of Liu et al. (2007). We have used the green band (558 nm) AOD and regridded the MISR data to model resolution for the analysis.

AERONET Level 2 aerosol product: The cloud-screened and quality-assured Level 2 AERONET direct AOD measurements were used in this study. Over India, there were five AERONET sites with Level 2 data for 2012 (accessed at <http://aeronet.gsfc.nasa.gov>). Four of the five stations are either in IGP or very close to it and one in SI as shown in Figure 1. The daily averaged AERONET observations were matched to the nearest GEOS-Chem grid cells at $0.5^\circ \times 0.667^\circ$ resolution. The spectral variation of measured AOD was also used to parse the measured AOD into a bimodal size distribution of fine and CM particles using the Spectral Deconvolution Algorithm developed by O’Neill et al. (2003). The fine and CM AOD values at 500 nm from the AERONET Spectral Deconvolution Algorithm were converted to those at 550 and 558 nm using the Ångström equation (to enable comparison with MODIS and MISR, respectively). The FM ($PM_{2.5}$) AOD in the model was determined by combining optical depth of inorganic aerosol, BC, OC, SSa, and four bins for dust (0.15–0.8 μm radii). The CM AOD was determined from SSc and three bins for dust (1.5–4.0 μm radii).

3.3. Methodology

Aerosols are short-lived species that are highly variable in space and time. Diurnal variations of AODs of 20–25% have been previously observed from the ground (AERONET stations) (Smirnov et al., 2002). Most of the available emission inventories (e.g., SMOG and MIX used here) are not dependent on time of day and provide averages for a day/month. Only factors such as chemical production, deposition, and transport are time dependent in the simulated values. Therefore, comparison of observations made at specific times and locations with model outputs that are of coarser spatial and temporal resolution is not significant. While the observations are snap shots (when the satellite flies over or when AERONET stations take their data), we compare them with the daily averaged model calculations. Hence, we present the median and mean values (for a season or year) along with measures of variability to compare observations with model outputs.

The raw calculated values can also be compared with individual observations. We have done so by calculating the mean bias (MB) of the model relative to the observations, as well as the regression slopes of calculated versus observed values. The mean bias is defined as

$$MB = \frac{1}{N} \sum_{i=1}^N (\text{Mod}_i - \text{Obs}_i)$$

where N is the number of model-observation intercomparisons and Mod_i and Obs_i are the i th modeled and observed values, respectively. Here a positive model bias indicates that the model prediction exceeds the observation. Such comparisons have to be tempered with the knowledge that we are dealing with a short-lived species with high spatial and temporal variability. A detailed accounting of the statistically analyzed information is given in the supporting information.

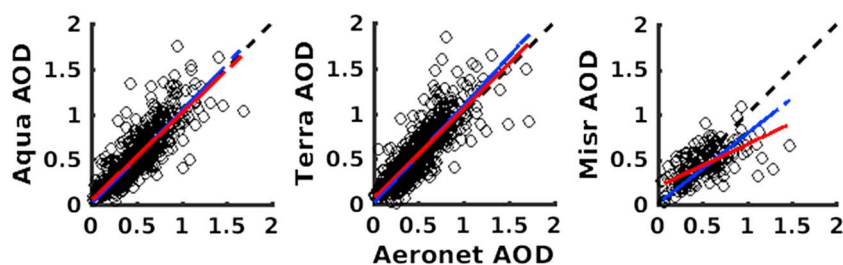


Figure 2. Scatter plot of Moderate Resolution Imaging Spectroradiometer (Aqua and Terra, 550 nm) and Multi-angle Imaging SpectroRadiometer (MISR) (558 nm) with Aerosol Robotic Network (AERONET) aerosol optical depth (AOD) (550 nm). The linear regression line is shown in red. The regression line with zero intercept is shown in blue. The black dashed line corresponds to slope = 1.

4. Results and Discussion

4.1. AOD Over India

In the following sections, we first compare available AOD observations from AERONET stations with those from satellites. Next, we compare observations of AOD data from different satellites. The measurement comparison aims to provide an assessment of the differences and variability between observations. Finally, we compare the observed AOD with those simulated in this study.

4.1.1. Comparison of AERONET AOD With MODIS (Aqua/Terra) and MISR

In Figure 2, we compare AOD from satellites (MODIS and MISR) with those measured by AERONET (daytime average) at 550 nm (MODIS) and 558 nm (MISR) at five locations (shown in Figure 1) for 2012. Note that the satellite does not exactly pass over the AERONET station all the time. Therefore, we compared the AERONET data against those measured by the satellite in areas of roughly 50×60 km around the AERONET station to enhance the number of available observations. One could also compare the AERONET data for the time of the satellite overpass or with those averaged for that particular day; but such a comparison would further reduce coincidences. The slope, correlation coefficient (R), intercept, and number of data points for MODIS (Aqua and Terra) and MISR measurements versus AERONET for $\text{AOD} \leq 2.0$ are given in Table S1 in the supporting information (discussed in section S2) for daily averages and for the time of the satellite overpass. The observed AOD (daily averaged and at the time of the satellite overpass) from MODIS agrees quite well with those from the five AERONET stations with slopes of ≥ 0.93 and $R \geq 0.83$. On average the MISR observations are lower than AERONET (mean bias = 0.07 ± 0.20), but the bias is not statistically different from zero. This comparison provides a rough measure of the agreement between observations so that we can keep these agreements/differences under consideration when comparing observations with our model calculations.

4.1.2. Comparison of GEOS-Chem Simulated AOD With Satellite and AERONET Observations

The GEOS-Chem model was run using emission inventories currently used in the model (details in section 3.1, referred as GC) and the newly developed SMOG inventory. Comparisons of the daily simulated AOD using both inventories with satellite observation from MODIS (Aqua and Terra) and MISR are detailed in the supporting information (section 3.1). In general, the simulated AOD at 550 nm was lower than those measured. Linear regressions that forced the lines through the origin showed that the calculated AODs were approximately 80% and 60% of those measured when using the SMOG and GC emission inventories, respectively (Figures S2 and S3 in the supporting information). Given the uncertainties in the measurements and variability in the aerosol, the simulated and observed AOD values compare reasonably well. However, a linear regression where the line is not forced through the origin suggests a bias, that is, a finite calculated value when the measured value is zero (see Table 2 and section S3.1 in the supporting information for details). We also observe a small seasonal variation in the correlations (Table S3 in the supporting information). Lastly, our calculated results agree slightly better with MISR than with MODIS (Table S2 in the supporting information).

The simulated AOD (using SMOG and GC emission inventories) was compared with AERONET observations (from five locations) at 440 nm, 500 nm, and 1,020 nm, and the slope, correlation coefficient, and intercept values are given in Table 1. The key points to note are as follows: (1) the model greatly underpredicts AOD at longer wavelengths (where contributions of coarser particles become more important) and (2) the model simulations using the SMOG inventory compare better with the observations than those using the GC

Table 1
The Slope, Correlation Coefficient (*R*), and Intercept (*c*) of Simulated AOD (Using SMOG and GC) Inventories With Five AERONET Observations

| Wavelength (nm) | SMOG | | | GC | | |
|----------------------------|-------------|----------|-------------|-------------|----------|-------------|
| | Slope | <i>R</i> | <i>c</i> | Slope | <i>R</i> | <i>c</i> |
| 440 | 0.65 ± 0.03 | 0.58 | 0.23 ± 0.02 | 0.47 ± 0.02 | 0.58 | 0.17 ± 0.01 |
| 500 | 0.56 ± 0.03 | 0.56 | 0.22 ± 0.02 | 0.39 ± 0.02 | 0.56 | 0.17 ± 0.01 |
| 1,020 | 0.20 ± 0.01 | 0.53 | 0.10 ± 0.00 | 0.18 ± 0.01 | 0.55 | 0.07 ± 0.00 |
| <i>With zero intercept</i> | | | | | | |
| 440 | 0.95 ± 0.01 | 0.91 | 0 | 0.69 ± 0.01 | 0.91 | 0 |
| 500 | 0.87 ± 0.01 | 0.91 | 0 | 0.63 ± 0.01 | 0.90 | 0 |
| 1,020 | 0.44 ± 0.01 | 0.89 | 0 | 0.35 ± 0.01 | 0.89 | 0 |

Note. AOD = aerosol optical depth; SMOG = Speciated Multi-pollutant Generator; GC = GEOS-Chem; AERONET = Aerosol Robotic Network.

inventory. As noted later, this difference between the inventories is mostly because of the larger OC and BC AOD simulated by the SMOG inventory that is discussed in the following section. Detailed comparisons of the monthly values are given in the supporting information (section S3.2).

4.2. Variation in Calculated AOD Between the Emission Inventories

The simulated AOD values at 550 nm using the SMOG and GC emission inventories are plotted in Figure 3. A linear regression yields a slope, correlation coefficient, and intercept of 1.3, 0.98, and -0.003 , respectively. The simulated AOD using SMOG is higher than that based on the GC inventory by $\sim 30\%$.

The SMOG and GC emission inventories differ with regard to primary combustion aerosol emissions (BC and OC) and SO_2 . The monthly SO_2 , BC, and OC emissions from SMOG and GC inventories over India are given in Table S7 in the supporting information. The detailed contributions of inorganic aerosol, BC, and OC optical depth to the calculated monthly AOD using SMOG and GC are given in Table S8 in the supporting information. The variation of these components across different regions of India is given in Figure 4a and Table 2. Figure 4b shows the OC and BC contributions to AOD calculated using the two inventories over the six regions. The figure and table show that the SMOG inventory gives higher BC and OC AOD compared to the GC inventory with higher values over the IGP. SMOG also gives a slightly higher inorganic aerosol AOD. As expected, dust and sea-salt AODs are essentially the same between the simulations. The higher OC AOD when using SMOG also leads to higher FM aerosols, as discussed below.

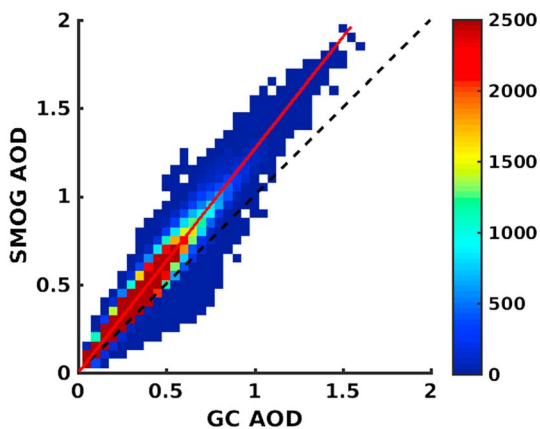


Figure 3. Density plot of simulated aerosol optical depth (AOD) (at 550 nm) using Speciated Multi-pollutant Generator (SMOG) and GEOS-Chem (GC) emission inventories at a horizontal resolution of $0.5^\circ \times 0.667^\circ$ for 2012. The linear regression line is shown in red. The color bar represents the number of data points in each 0.05 AOD bin.

4.3. Evaluation of FM and CM AOD

The simulated FM and CM AOD (using SMOG and GC) at 500 nm are compared with the AERONET observations for $\text{AOD} \leq 2.0$ and shown in Figure 5; the slope, correlation coefficient, and intercept are given in Table 3. The simulated FM AOD using SMOG was higher compared to GC. Overall, the calculated FM AOD is in reasonable agreement with the AERONET data (slope = 1.1 and $R = 0.86$ with SMOG; see Table 3 for more details). However, it is also clear from the figure that our model is underestimating the large particles, and as discussed below (section 4.4), we attribute the difference to inadequate representation of dust over India. It is worth noting that Philip et al. (2017) have estimated that inclusion of anthropogenic fugitive, combustion, and industrial dust emissions in GEOS-Chem reduced the model bias in $\text{PM}_{2.5}$ from 17% to 7% over East and South Asia in comparison with Surface PM Network measurements.

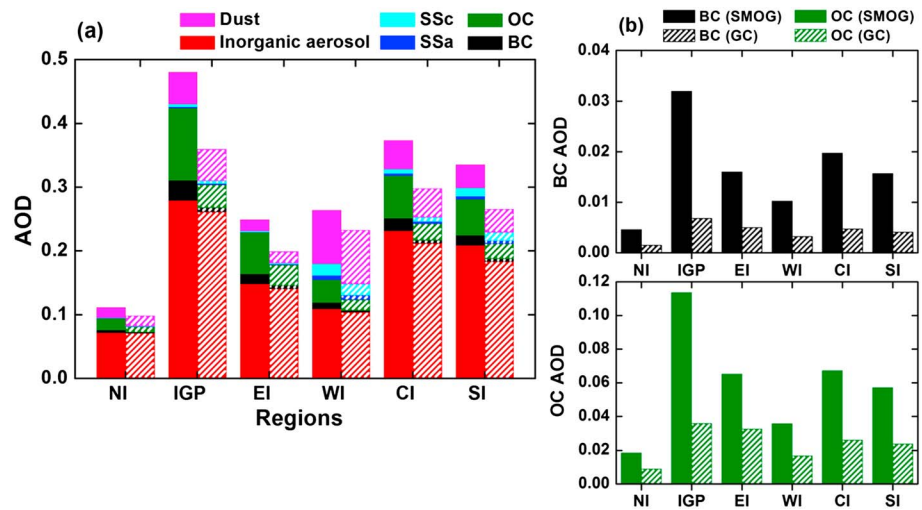


Figure 4. (a) The variation of aerosol optical depth (AOD) over the six regions in India. The contribution of inorganic aerosol, black carbon (BC), organic carbon (OC), accumulation sea salt (SSa), coarse-mode sea salt (SSc), and dust AOD (at 550 nm) to the simulated total AOD using Speciated Multi-pollutant Generator (SMOG) (solid) and GEOS-Chem (GC) (hatched) emission inventories and (b) contributions of OC and BC to calculated AOD from the two emission inventories over the six Indian regions.

4.4. Dust May Be an Important Aerosol Component Over the Entire Indian Subcontinent

To have a better understanding of the CM AOD in our model, the simulated dust AOD (at 550 nm) was compared with the dust AOD (at ~558 nm) from the MISR measurements over India. The dust AOD in the model is determined by combining the optical depth from the seven bins for dust as mentioned in section 3.1. The dust size range in the model is 0.10–4.0 μm (radius). MISR considers dust in the size range 0.10–6.0 μm (radius). More details on the MISR dust components are given by Kahn et al. (2010). GEOS-Chem underestimates dust AOD compared to MISR by a factor of 5 or more. The dust AOD was further analyzed over the six regions specified in section 2, with the resulting box and whisker plot shown in Figure 6. The simulated dust AOD was underestimated over all the regions with the exception of WI, which is mostly a desert. MISR AOD is reasonable for low-to-medium aerosol loadings over dust-affected areas. It is probably underestimated in high dust events due to reduced sensitivity to surface reflectance and angular shape. The current v22 MISR aerosol climatology lacks plate-like and strong absorbent dust particles as well as certain mixtures, such as medium, spherical, absorbing particles combined with dust, which can lead to an underestimation of dust AOD (Kahn et al., 2010; Kalashnikova et al., 2005). Therefore, the MISR dust AOD in Figure 6 is a lower limit, which suggests that the differences between observations and our model for dust might be even larger than what is shown in the figure.

Table 2
The Calculated Contribution of Aerosol Components (in Percentage) to Total AOD at 550 nm Over the Six Regions in India

| Regions | Aerosol components (%) | | | | | |
|---------|------------------------|----|----|-----|-----|------|
| | Inorganic aerosol | BC | OC | SSa | SSc | Dust |
| SMOG | | | | | | |
| NI | 64 | 4 | 17 | 0.3 | 0.4 | 14 |
| IGP | 58 | 7 | 24 | 0.4 | 0.9 | 10 |
| EI | 60 | 6 | 26 | 0.4 | 0.7 | 7 |
| WI | 41 | 4 | 14 | 3 | 7 | 32 |
| CI | 62 | 5 | 18 | 0.9 | 2 | 12 |
| SI | 62 | 5 | 17 | 1 | 4 | 11 |
| GC | | | | | | |
| NI | 72 | 2 | 9 | 0.3 | 0.5 | 16 |
| IGP | 73 | 2 | 10 | 0.6 | 1 | 14 |
| EI | 71 | 3 | 16 | 0.5 | 1 | 9 |
| WI | 45 | 1 | 7 | 3 | 8 | 36 |
| CI | 71 | 2 | 9 | 1 | 2 | 15 |
| SI | 69 | 2 | 9 | 2 | 5 | 14 |

Note. These calculations used the SMOG and GC inventories. Clearly, inorganic aerosol is the major contributor across India. AOD = aerosol optical depth; BC = black carbon; OC = organic carbon; SSa = accumulation sea salt; SSc = coarse-mode sea salt; SMOG = Speciated Multi-pollutant Generator; NI = Northern India; IGP = Indo-Gangetic Plain; EI = Eastern India; WI = Western India; CI = Central India; SI = Southern India; GC = GEOS-Chem. The numbers do not add up to exactly 100% because of rounding off errors.

Our comparisons of simulated AOD with AERONET AOD (Figures 5 and 6) show that overall our model underestimates dust AOD over most of India. It is possible that part of the difference comes from transport of dust that is not captured in our model. However, the observations and processes not included in the model strongly suggest that there is a significant amount of nondesert dust in other parts of India (Philip et al., 2017). Models are unlikely to capture the dust kicked up from the surface or generated by various anthropogenic activities, some of which could be unique to India. Quantification of such sources of dust would require detailed measurements of aerosol composition as a function of

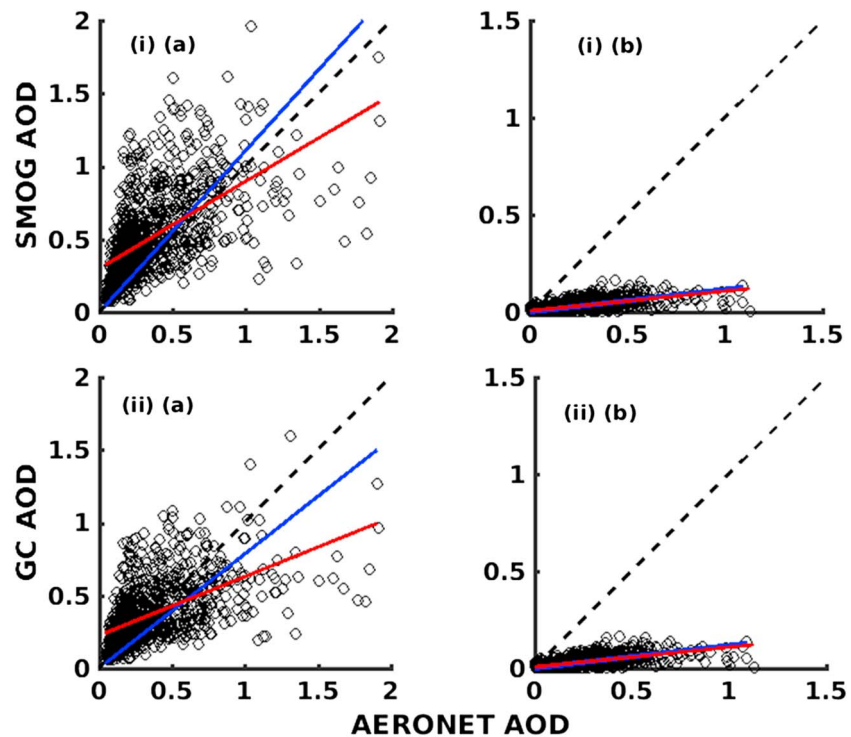


Figure 5. The scatter plot of simulated (a) fine-mode and (b) coarse-mode aerosol optical depth (AOD) at 500 nm with Aerosol Robotic Network (AERONET) observations using (i) Speciated Multi-pollutant Generator (SMOG) and (ii) GEOS-Chem (GC) emission inventories. The linear regression line is shown in red. The regression line with zero intercept is shown in blue. The black dashed line corresponds to slope = 1.

season in various parts of India and representation of those processes in GEOS-Chem and other models. In addition, a large number of ground stations, such as the Aerosol Radiative Forcing over India network (Babu et al., 2013) would greatly help in identifying and quantifying dust over all the parts of India.

4.5. Seasonal Variation in AOD Over India Is Not Very Large

The comparison of simulated AOD (using SMOG and GC) with satellite and observations showed that (1) simulated AOD was higher when using the SMOG emission inventory, (2) month-to-month variations in AOD, and (3) regional differences in AOD over India. In this section, we will discuss the seasonal variation in simulated AOD (using SMOG) relative to satellite (MODIS and MISR) and AERONET measurements over the six regions.

Table 3
The Slope, Correlation Coefficient (R), and Intercept (c) of Simulated FM and CM AOD (Using SMOG and GC Inventories) at 500 nm With AERONET Observations

| | SMOG | | | GC | | |
|----------------------------|-------------|------|-------------|-------------|------|-------------|
| | Slope | R | c | Slope | R | c |
| FM | 0.60 ± 0.03 | 0.59 | 0.30 ± 0.01 | 0.41 ± 0.02 | 0.56 | 0.23 ± 0.01 |
| CM | 0.10 ± 0.00 | 0.67 | 0.01 ± 0.00 | 0.10 ± 0.00 | 0.67 | 0.01 ± 0.00 |
| <i>With zero intercept</i> | | | | | | |
| FM | 1.1 ± 0.02 | 0.86 | 0 | 0.79 ± 0.02 | 0.85 | 0 |
| CM | 0.12 ± 0.00 | 0.84 | 0 | 0.12 ± 0.00 | 0.84 | 0 |

Note. FM = fine mode; CM = coarse mode; AOD = aerosol optical depth; SMOG = Speciated Multi-pollutant Generator; GC = GEOS-Chem; AERONET = Aerosol Robotic Network.

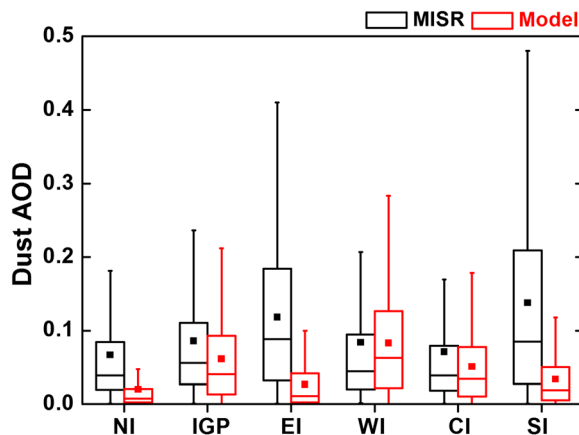


Figure 6. Box and whisker plot of dust aerosol optical depth (AOD) at ~550 nm from Multi-angle Imaging SpectroRadiometer (MISR) and simulated (using Speciated Multi-pollutant Generator) over the six regions. In the box plot, the inside line and square is the median and mean, respectively. Box boundaries are 25th–75th percentiles, and whiskers indicate the 5th and 95th percentiles.

The simulated AOD at 440 nm, 500 nm, and 1020 nm was compared with the AERONET observations as box and whisker plots; results are shown in Figure 7. Overall, the AOD does not vary significantly across the four seasons. The highest AOD values were observed in the postmonsoon months. The seasonal mean AOD (440 nm and 500 nm) values were comparable for summer and winter seasons (within 6%), and the simulated values are in agreement with satellite observations (Figure 8), which was within ~4–9% relative to Terra. During monsoon, the mean AOD (440 and 500 nm) was underestimated by ~15–23%. The mean AOD at 1020 nm was underestimated in all the seasons by ~34–62%.

Figure 8 shows a box and whisker plot of mean AOD (we have considered AOD values ≤ 2.0) from the model and satellite measurements for the four seasons. The mean AOD values for the different seasons varied among the satellite measurements. Again, it is evident from the figure that the AOD does not vary drastically between the seasons. The figure also shows that on average, both the model and satellite measurements indicate high AOD in summer (SMOG: 0.427, Aqua: 0.380, Terra: 0.443, and MISR: 0.417) with the differences between these data sets of 2–12%. Our model overestimated AOD values by ~8–10% relative to

Terra in the postmonsoon period (SMOG: 0.470, Aqua: 0.358, Terra: 0.437, and MISR: 0.320) and winter (SMOG: 0.395, Aqua: 0.296, Terra: 0.361, and MISR: 0.285). During monsoon, the model underestimated the AOD values (CE: 0.320, Aqua: 0.422, Terra: 0.507, and MISR: 0.368) by ~24–37% relative to MODIS and ~13% relative to MISR. More details on the seasonal variation of simulated AOD relative to satellite observations over the six regions are given in section S5 in the supporting information. The model overestimated AOD over CI and SI relative to the satellite observations in all seasons outside of the monsoon (Figure S4 in the supporting information).

4.6. Spatial Distribution of AOD Over the Indian Subcontinent

We have shown above that our model underestimates the dust AOD while reasonably reproducing other components. Therefore, we have added the AOD due to dust to the calculated total AOD values from the model. As noted above, the extent of underestimation of dust AOD varies with season. Unfortunately, we do not have enough AERONET stations to evaluate the underestimation of dust AOD (e.g., calculated as the ratio of CM AOD between AERONET and the model) in different regions of India; indeed, four out of five stations are essentially in the IGP. By assuming that the underestimation of dust AOD over all of India is similar to that seen over IGP, we have corrected our calculated AOD according to the factors shown in Table 4 (note: factors are applied only to size bins 5, 6, and 7). Correcting the model in this way leads to an increase in the corrected mean AOD (at 550 nm) over WI by as much as a factor of 2 and between 16 and 39% over the other

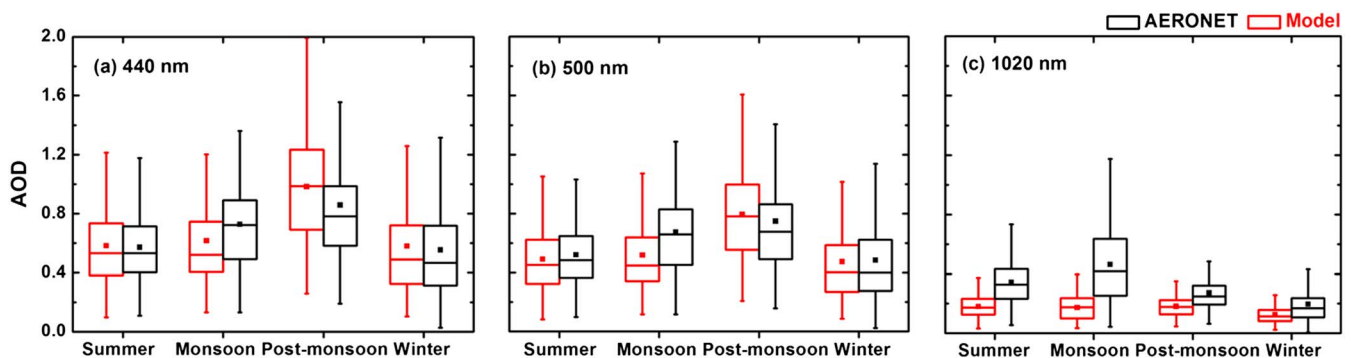


Figure 7. Box and whisker plot of mean aerosol optical depth (AOD) from model (using Speciated Multi-pollutant Generator) and Aerosol Robotic Network (AERONET) for the four seasons. In the box plot, the inside line and square are the median and mean, respectively. Box boundaries are 25th–75th percentiles, and whiskers indicate the 5th and 95th percentiles.

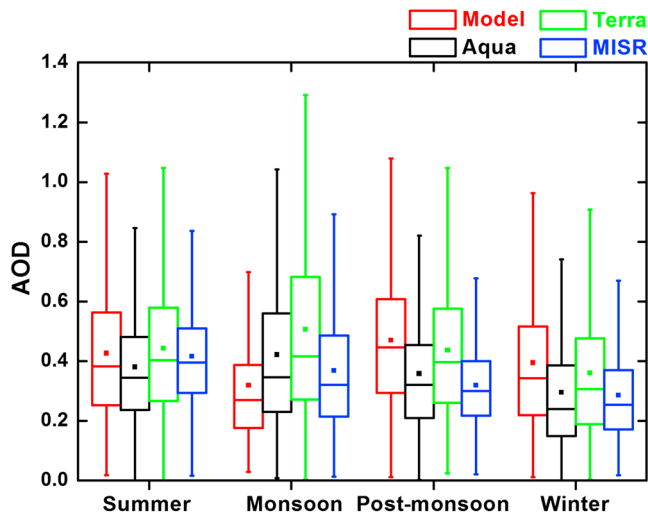


Figure 8. Box and whisker plot of mean aerosol optical depth (AOD) at 550 nm from model (using Speciated Multi-pollutant Generator) and satellite (Moderate Resolution Imaging Spectroradiometer and Multi-angle Imaging SpectroRadiometer (MISR)) for the four seasons. In the box plot, the inside line and square are the median and mean, respectively. Box boundaries are 25th–75th percentiles, and whiskers indicate the 5th and 95th percentiles.

regions in comparison to the simulated AOD in the baseline simulation. Of course, information about dust AOD over other parts of India would be very beneficial. Table S8 in the supporting information gives the total AOD before and after multiplication by the seasonal correction factors shown in Table 4. It shows that this correction does not greatly alter the calculated overall AOD values.

The spatial distribution of monthly averaged AOD (corrected for dust) over India is compared with satellite observations (Aqua, Terra, and MISR) in Figure 9. The equivalent figure without correction for dust is included in the supporting information (Figure S5). The general features of the observed spatial variation are also seen in the model calculations. A few key spatial features stand out in calculated values and in the observations: (1) the IGP, as expected, has higher AOD levels than most other parts of India. This is to be expected given the higher population density and larger emission sources in the region and (2) the spatial distribution of the calculated AOD varies in accordance with the emission sources, modulation by meteorological conditions, wet removal associated with the monsoon, and seasonal variation of dispersion. During the winter season (December–February), the aerosol loading is dominated by the anthropogenic contribution, with higher loading in northern India compared to the peninsular region (Tripathi et al., 2006). We see the highest AOD over the IGP followed by EI, southwestern India, and east coast-northern Bay of Bengal region; this observa-

tion is also consistent with satellite observations. The maximum AOD occurs over central and eastern IGP coinciding with the locations of coal-based thermal power plants. Our model also captures the continental outflow over the northern Bay of Bengal. The topography along with meteorology (low wind) is conducive for the accumulation of AOD over this region. In addition, over the IGP the pollutants are trapped in the shallow atmospheric boundary layer leading to hazy conditions during this period. The simulated AOD agrees with satellite observations for all regions except CI and SI. Our model overestimates AOD values over CI and SI when using the SMOG emission inventory.

In the summer months (March–May), we see an increase in AOD over India. Previous studies have suggested that transport of mineral dust from Arabian and Thar deserts by westerly winds (Dey et al., 2004; Sijkumar et al., 2016) may lead to enhanced AOD. High AOD values over northwestern India, IGP, and the west and southwest coast are observed by MODIS and MISR. However, the MODIS values are higher than those of MISR. Our model simulates high AOD over all regions except northwestern India, which can be attributed to the low dust AOD in our model as discussed in section 4.4.

Srivastava et al. (2012) have shown that the dust contribution to total AOD during this period was ~62% over Kanpur. Except for WI, our model simulated AOD is within ~20% of the satellite observations.

During monsoon, the high AOD over northwest India and northern Arabian Sea may be associated with the strong westerly winds that could transport dust from the Arabian Desert; it is interesting to note that such enhanced values are also observed by MODIS and MISR. The MODIS-derived monthly mean AOD values are much higher compared to MISR; the difference may be partly associated with the retrieval algorithm. The AOD spatial distribution is well simulated by our model, indicating that the model is generally able to capture the relevant transport features. As noted earlier, dust is underestimated in our model, possibly because there are emissions that are not accounted for in the current inventories, for example, dust from transportation and land use methods. We did not attempt to identify the specific contributions due to dust transport from outside of the Indian region. Such an attribution study would be beneficial.

Table 4
Monthly Correction Factors Applied to Dust AOD (Size Bins 5, 6, and 7) Simulated for 2012

| Month | Factor multiplied to dust AOD |
|-----------|-------------------------------|
| January | 6 |
| February | 6 |
| March | 7 |
| April | 5 |
| May | 8 |
| June | 9 |
| July | 9 |
| August | 7 |
| September | 13 |
| October | 13 |
| November | 30 |
| December | 37 |

Note. AOD = aerosol optical depth.

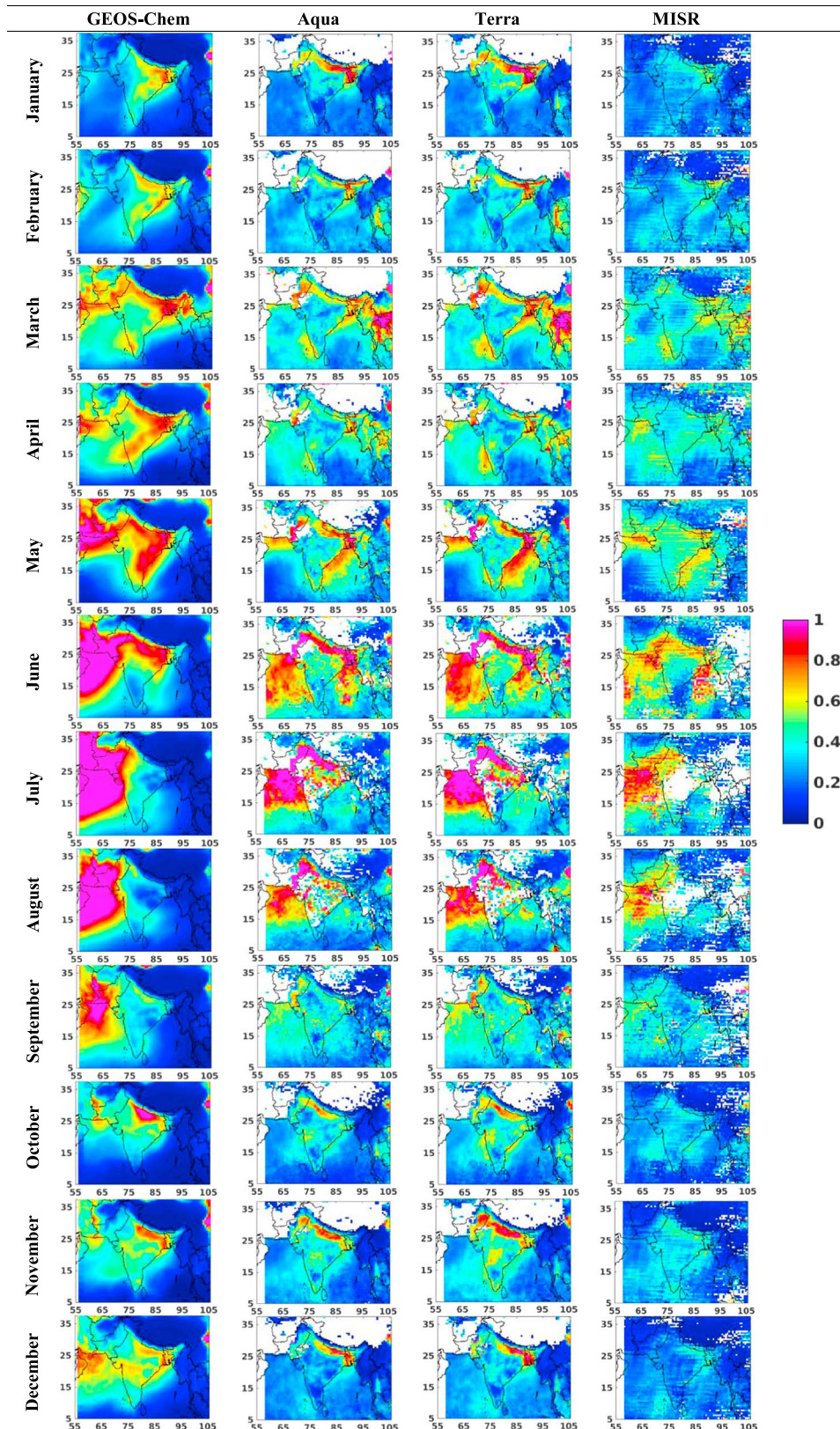


Figure 9. Spatial variation of aerosol optical depth at 550 nm (after dust correction) from Goddard Earth Observing System (GEOS)-Chem (using Speciated Multi-pollutant Generator), Moderate Resolution Imaging Spectroradiometer (Aqua and Terra), and Multi-angle Imaging SpectroRadiometer (MISR). The color bar represents the aerosol optical depth values.

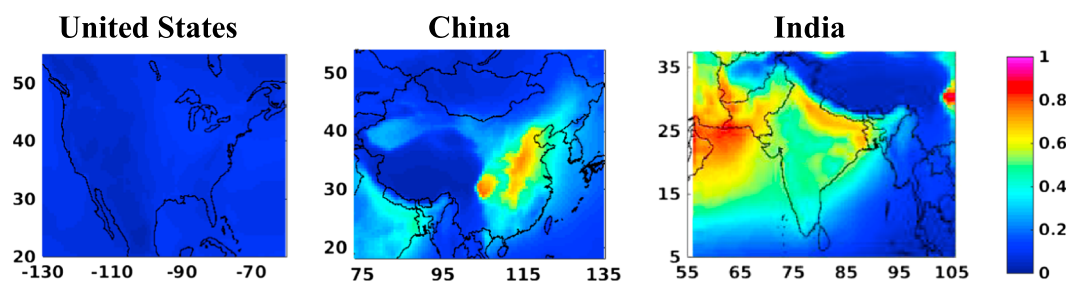


Figure 10. Simulated mean aerosol optical depth at 550 nm over the United States, China, and India for 2012. The color bar represents the aerosol optical depth values. AOD over China (middle panel) was calculated using GC inventory, while that over India (right panel) used SMOG inventory.

In the postmonsoon season, the southwesterly winds weaken and reduce the dust transport to the Indian subcontinent. From the satellite observations, it is evident that AOD was high along the IGP associated with agricultural burning over the northwest IGP. During this time the winds are northwesterly, which transports aerosols to the central and eastern IGP. The nested GEOS-Chem model captured these features. Our model also simulated high AOD over few cities (between 15° and 25°N) that coincide with enhancements seen in the satellite observations.

4.7. An Integrated View of Aerosols and Their Composition Over India

Figure 1 shows the variation of AOD (at 550 nm without dust correction) over the six regions of India as calculated in this study. Here the area of the pie represents the total AOD and the fractional contributions from various sources are shown as pieces of the pie. As it is well known, IGP has the highest AOD among all the regions of India. The cleanest region is NI, with an average AOD ~23% of that over IGP. Interestingly, CI and SI also have significant aerosol loading. Even though emissions are much lower in EI, there is a significant level of aerosols due to transport from IGP and possibly CI. Conversely, NI does not appear to be influenced to any significant extent by emissions in IGP.

Another key feature of the distribution of the aerosols across India is their composition (see Table 2). As expected, WI has relatively large contribution from dust and sea salt. Indeed, the contribution of dust is comparable to that of inorganic aerosols (anthropogenic). In all the other regions, inorganic aerosols are the major component, with little contribution from sea salt. EI (which is much less developed) has the highest levels of OC and BC. It is important to note that the sum of OC and BC (Table 2), related to various activities such as wood (for cooking), trash, and agricultural burning, contributes ~18–32% to the total AOD over much of India. The inorganic aerosols, OC, and BC are mostly in the FM, and they are predominantly anthropogenic in origin. Therefore, it is clear that anthropogenic aerosols, which are amenable to reduction by human interventions, dominate every region of India.

It would be very beneficial to compare our calculated aerosol composition with observations. Such a comparison would help ascertain the validity of the emission inventories and the ability of the model to capture aerosol composition over India. There are various measurements of the components of aerosols from various campaigns and stations (George et al., 2008, 2011; Kumar et al., 2016; Singh et al., 2016). Measurements have shown that BC is a large contributor in megacities and large cities. Various measurements also show that there are significant amounts of sulfate and nitrate aerosols. Many measurements have shown the prevalence of dust (Dey et al., 2004; Misra et al., 2014; Sijikumar et al., 2016). However, there is no comprehensive data for any of the locations to examine and compare our calculated composition with observations. This issue is further exacerbated by the rapid change in emissions, which makes it difficult to compare the calculated values for 2012 with the available observations. It will be very useful to develop a comprehensive data set on aerosol composition over India and the associated changes with time.

4.8. Comparison With AOD Observations Over the United States and China

It has been recognized over past decades that aerosol pollution in India is very high. To provide a context for the pollution levels, we compare the simulated mean AOD for 2012 over India to those over the United States and China in Figure 10. Clearly, aerosol loading over India is comparable to many of the polluted regions over China and much larger than over the United States, where pollution controls have been in place for decades.

This finding is not new but underlines the point that AOD over most regions of India is a factor of 5 or more than over the United States. The majority of the difference is due to much larger emissions of primary aerosols and precursors of secondary aerosols. The extent of transport of aerosols (except dust) from other regions is expected to be small for India. Our calculated AOD over India can be compared to those calculated over the United States and China using GEOS-Chem, and this large difference is borne out. Comparison of GEOS-Chem ($0.5^\circ \times 0.667^\circ$ resolution) with AERONET stations over the United States gave a slope and correlation coefficient of 0.75 and 0.84, respectively (Li et al., 2013). Over China, the daily values gave a correlation coefficient of 0.6 and slope of 0.41 (Li et al., 2016).

The seasonal mean AOD over the United States from MISR data is <0.2 with maximum values reaching ~ 0.25 over central United States and parts of the East Coast in summer (Figure S6a, supporting information). Over China, the northwest region (Taklimakan desert) is a source of natural aerosols dominated by desert dust and the North China Plain and south China are sources of anthropogenic aerosol with mean AOD values in the range 0.4–0.6 (Figure S5b, supporting information). The low AOD regions are located in areas with high vegetation cover and sparse population in the high-latitude regions in northeast China with AOD about 0.2 and high-altitude regions in southwest China with AOD ~ 0.1 –0.2. The wintertime AOD is lowest in China. Spring-summer AOD maximum values were in the range 0.6–0.75 over the North China Plain. Over southern China, high AOD occurs before and after the Asian summer monsoon, a period of low AOD (Figure S5b, supporting information). Compared to the United States and China, the mean AOD over India is higher by a factor > 2 with the oceanic regions surrounding the Indian subcontinent having mean AOD > 0.35 . Seasonally, the mean AOD values are > 0.3 where the population resides and the minimum AOD values observed are > 0.25 . Again, these observations and our calculations suggest that India is currently one of the most polluted regions in terms of aerosols and no season has low concentrations of PM pollution.

5. Conclusions

In this study, the tropospheric column AOD simulated by a high-resolution nested version of GEOS-Chem was evaluated with satellite data (MODIS and MISR) and ground-based measurements (five AERONET sites) over India for 2012. The observations themselves were also intercompared. Our model simulations were driven with two emission inventories: GC (standard emission inventories used in the model) and SMOG (provided by IIT Bombay). The main results of the study are summarized below.

1. The AERONET data compared better with MODIS satellite data (with a slope and correlation coefficient of ≥ 0.96 and ~ 0.84 , respectively) than with the MISR data.
2. The calculated AOD values were $\sim 80\%$ (SMOG) and 60% (GC) of those measured by the satellite and exhibited slightly better agreement with MISR than with MODIS.
3. Comparison of simulated AOD with AERONET observations at 440 nm, 500 nm, and 1020 nm showed that the model underpredicted AOD at longer wavelengths while agreeing reasonably well at 440 and 550 nm. Simulations using SMOG agreed better with observations than did those using the GC emission inventory.
4. SMOG and GC inventories differ in the emission of aerosol precursor gases (BC, OC, and SO_2). The SMOG inventory has higher BC, OC, and inorganic aerosol levels compared to GC.
5. The GEOS-Chem model was capable of simulating FM AOD (responsible for $\text{PM}_{2.5}$ and hence impacts health) over India; however, there was an underestimation of CM particles by the model.
6. Dust is the major component underrepresented in the model over India with a possibility of significant nondesert dust over most parts of India, some of which is likely to be anthropogenic in origin.
7. The model captured the general features of spatial variation of AOD (after dust correction) at 550 nm seen in the satellite observations (Aqua, Terra, and MISR).
8. We provide a comprehensive view of the aerosol amounts and composition over different regions in India divided according to meteorology.
9. We have shown that IGP is a highly polluted region. Most other Indian regions are also polluted, with Northern India being the least polluted. We also show that EI is greatly influenced by emissions from IGP.

References

- Babu, S. S., Manoj, M. R., Moorthy, K. K., Gogoi, M. M., Nair, V. S., Kompalli, S. K., et al. (2013). Trends in aerosol optical depth over Indian region: Potential causes and impact indicators. *Journal of Geophysical Research: Atmospheres*, 118, 11,794–11,806. <https://doi.org/10.1002/2013JD020507>

Acknowledgments

We thank the Aqua/MODIS and Terra/MODIS Aerosol Product 5 min L2 Swath 10 km, C6, NASA Level-2 and Atmosphere Archive and Distribution System (LAADS) Distributed Active Archive center (DAAC) Goddard Space Flight Center, Greenbelt, MD (<https://ladsweb.nascom.nasa.gov/>). The MISR data were obtained from the NASA Langley Research Center Atmospheric Science Data Center. We thank the principal investigators (PI) and their staff for establishing and maintaining the AERONET sites used in this investigation. We are grateful to Ralph Kahn for useful pointers and discussions about MISR data. Special thanks to Matthew Bishop for downloading the GEOS-5 meteorological files. This work was funded by Colorado State University. Dylan B Millet and Sreelekha Chaliyakunnel acknowledge support from NASA (NNX14AP89G), NSF (AGS-1148951), and the Minnesota Supercomputing Institute. The modeled data are available from the authors upon request.

- Bay, I., Jacob, D. J., Yantosca, R. M., Logan, J. A., Field, B. D., Fiore, A. M., et al. (2001). Global modeling of tropospheric chemistry with assimilated meteorology: Model description and evaluation. *Journal of Geophysical Research*, *106*(D19), 23,073–23,095. <https://doi.org/10.1029/2001JD000807>
- Bond, T. C., Bhardwaj, E., Dong, R., Jogani, R., Jung, S., Roden, C., et al. (2007). Historical emissions of black and organic carbon aerosol from energy-related combustion, 1850–2000. *Global Biogeochemical Cycles*, *21*, GB2018. <https://doi.org/10.1029/2006GB002840>
- Boucher, O., Randall, D., Artaxo, P., Bretherton, C., Feingold, G., Forster, P., et al. (2013). Clouds and Aerosols. In T. F. Stocker, et al. (Eds.), *Climate change 2013: The physical science basis. Contribution of working group I to the fifth assessment report of the intergovernmental panel on climate change*. Cambridge, UK: Cambridge University Press.
- Chin, M., Chu, A., Levy, R., Remer, L., Kaufman, Y., Holben, B., et al. (2004). Aerosol distribution in the Northern Hemisphere during ACE-Asia: Results from global model, satellite observations, and Sun photometer measurements. *Journal of Geophysical Research*, *109*, D23590. <https://doi.org/10.1029/2004JD004829>
- Chin, M., Diehl, T., Dubovik, O., Eck, T. F., Holben, B. N., Sinyuk, A., & Streets, D. G. (2009). Light absorption by pollution, dust, and biomass burning aerosols: A global model study and evaluation with AERONET measurements. *Annales de Geophysique*, *27*(9), 3439–3464. <https://doi.org/10.5194/angeo-27-3439-2009>
- Central Pollution Control Board (2014). National ambient air quality status and trends-2012.
- de Meij, A., Pozzer, A., & Lelieveld, J. (2012). Trend analysis in aerosol optical depths and pollutant emission estimates between 2000 and 2009. *Atmospheric Environment*, *51*, 75–85. <https://doi.org/10.1016/j.atmosenv.2012.01.059>
- Dey, S., Tripathi, S. N., & Singh, R. P. (2004). Influence of dust storms on the aerosol optical properties over the Indo-Gangetic basin. *Journal of Geophysical Research*, *109*, D20211. <https://doi.org/10.1029/2004JD004924>
- Drury, E., Jacob, D. J., Spurr, R. J. D., Wang, J., Shinzuka, Y., Anderson, B. E., et al. (2010). Synthesis of satellite (MODIS), aircraft (ICARTT), and surface (IMPROVE, EPA-AQS, AERONET) aerosol observations over eastern North America to improve MODIS aerosol retrievals and constrain surface aerosol concentrations and sources. *Journal of Geophysical Research*, *115*, D14204. <https://doi.org/10.1029/2009JD012629>
- Fisher, J. A., Jacob, D. J., Wang, Q., Bahreini, R., Carouge, C. C., Cubison, M. J., et al. (2011). Sources, distribution, and acidity of sulfate-ammonium aerosol in the Arctic in winter-spring. *Atmospheric Environment*, *45*(39), 7301–7318. <https://doi.org/10.1016/j.atmosenv.2011.08.030>
- George, S. K., Nair, P. R., Parameswaran, K., & Jacob, S. (2011). Wintertime chemical composition of aerosols at a rural location in the Indo-Gangetic Plains. *Journal of Atmospheric and Solar - Terrestrial Physics*, *73*(13), 1798–1809. <https://doi.org/10.1016/j.jastp.2011.04.005>
- George, S. K., Nair, P. R., Parameswaran, K., Jacob, S., & Abraham, A. (2008). Seasonal trends in chemical composition of aerosols at a tropical coastal site of India. *Journal of Geophysical Research*, *113*, D16209. <https://doi.org/10.1029/2007JD009507>
- Giglio, L., Randerson, J. T., & Van Der Werf, G. R. (2013). Analysis of daily, monthly, and annual burned area using the fourth-generation global fire emissions database (GFED4). *Journal of Geophysical Research: Biogeosciences*, *118*, 317–328. <https://doi.org/10.1002/jgrg.20042>
- Giles, D. M., Holben, B. N., Tripathi, S. N., Eck, T. F., Newcomb, W. W., Slutsker, I., et al. (2011). Aerosol properties over the Indo-Gangetic Plain: A mesoscale perspective from the TIGERZ experiment. *Journal of Geophysical Research*, *116*, D18203. <https://doi.org/10.1029/2011JD015809>
- Ginoux, P., Chin, M., Tegen, I., Prospero, J. M., Holben, B., Dubovik, O., & Lin, S. J. (2001). Sources and distributions of dust aerosols simulated with the GOCART model. *Journal of Geophysical Research*, *106*(D17), 20,255–20,273. <https://doi.org/10.1029/2000JD000053>
- Granier, C., Bessagnet, B., Bond, T., D'Angiola, A., Denier van der Gon, H., Frost, G. J., et al. (2011). Evolution of anthropogenic and biomass burning emissions of air pollutants at global and regional scales during the 1980–2010 period. *Climatic Change*, *109*(1–2), 163–190. <https://doi.org/10.1007/s10584-011-0154-1>
- Guenther, A. B., Jiang, X., Heald, C. L., Sakulyanontvittaya, T., Duhl, T., Emmons, L. K., & Wang, X. (2012). The model of emissions of gases and aerosols from nature version 2.1 (MEGAN2.1): An extended and updated framework for modeling biogenic emissions. *Geoscientific Model Development*, *5*(6), 1471–1492. <https://doi.org/10.5194/gmd-5-1471-2012>
- Henriksson, S. V., Laaksonen, A., Kerminen, V. M., Räisänen, P., Järvinen, H., Sundström, A. M., & De Leeuw, G. (2011). Spatial distributions and seasonal cycles of aerosols in India and China seen in global climate-aerosol model. *Atmospheric Chemistry and Physics*, *11*(15), 7975–7990. <https://doi.org/10.5194/acp-11-7975-2011>
- Hu, L., Millet, D. B., Baasandorj, M., Grif, T. J., Turner, P., Helmig, D., et al. (2015). Isoprene emissions and impacts over an ecological transition region in the U.S. Upper Midwest inferred from tall tower measurements. *Journal of Geophysical Research: Atmospheres*, *120*, 3553–3571. <https://doi.org/10.1002/2014JD022732>
- Jaeglé, L., Quinn, P. K., Bates, T. S., Alexander, B., & Lin, J. T. (2011). Global distribution of sea salt aerosols: New constraints from in situ and remote sensing observations. *Atmospheric Chemistry and Physics*, *11*(7), 3137–3157. <https://doi.org/10.5194/acp-11-3137-2011>
- Jethva, H., Satheesh, S. K., & Srinivasan, J. (2007). Assessment of second-generation MODIS aerosol retrieval (Collection 005) at Kanpur, India. *Geophysical Research Letters*, *34*, L19802. <https://doi.org/10.1029/2007GL029647>
- Kahn, R. A., Gaitley, B. J., Garay, M. J., Diner, D. J., Eck, T. F., Smirnov, A., & Holben, B. N. (2010). Multiangle imaging Spectroradiometer global aerosol product assessment by comparison with the Aerosol Robotic Network. *Journal of Geophysical Research*, *115*, D23209. <https://doi.org/10.1029/2010JD014601>
- Kalashnikova, O. V., Kahn, R., Sokolik, I. N., & Li, W. H. (2005). Ability of multiangle remote sensing observations to identify and distinguish mineral dust types: Optical models and retrievals of optically thick plumes. *Journal of Geophysical Research*, *110*, D18514. <https://doi.org/10.1029/2004JD004550>
- Kar, J., Deeter, M. N., Fishman, J., Liu, Z., Omar, A., Creilson, J. K., et al. (2010). Wintertime pollution over the Eastern Indo-Gangetic Plains as observed from MOPITT, CALIPSO and tropospheric ozone residual data. *Atmospheric Chemistry and Physics*, *10*(24), 12,273–12,283. <https://doi.org/10.5194/acp-10-12273-2010>
- Kaufman, Y. J., Tanr, D., Remer, L. A., Vermote, E. F., & Chu, A. (1997). Operational remote sensing of tropospheric aerosol over land from EOS moderate resolution imaging spectroradiometer after the launch of MODIS the distribution. *Journal of Geophysical Research*, *102*(D14), 17,051–17,067. <https://doi.org/10.1029/96JD03988>
- Koepke, P., Hess, M., Schult, I., & Shettle, E. P. (1997). Global Aerosol Data Set, report no. 243, max-Planck-Institut für Meteorologie, Hamburg.
- Kumar, B., Chakraborty, A., Tripathi, S. N., & Bhattu, D. (2016). Highly time resolved chemical characterization of submicron organic aerosols at a polluted urban location. *Environmental Science: Processes & Impacts*, *18*(10), 1285–1296. <https://doi.org/10.1039/C6EM00392C>
- Lau, K. M., Kim, M. K., & Kim, K. M. (2006). Asian summer monsoon anomalies induced by aerosol direct forcing: The role of the Tibetan Plateau. *Climate Dynamics*, *26*(7–8), 855–864. <https://doi.org/10.1007/s00382-006-0114-z>
- Levy, R. C., Mattoo, S., Munchak, L. A., Remer, L. A., Sayer, A. M., Patadia, F., & Hsu, N. C. (2013). The Collection 6 MODIS aerosol products over land and ocean. *Atmospheric Measurement Techniques*, *6*(11), 2989–3034. <https://doi.org/10.5194/amt-6-2989-2013>
- Levy, R. C., Remer, L. A., Kleidman, R. G., Mattoo, S., Ichoku, C., Kahn, R., & Eck, T. F. (2010). Global evaluation of the Collection 5 MODIS dark-target aerosol products over land. *Atmospheric Chemistry and Physics*, *10*(21), 10,399–10,420. <https://doi.org/10.5194/acp-10-10399-2010>

- Li, M., Zhang, Q., Kurokawa, J., Woo, J. H., He, K. B., Lu, Z., et al. (2017). MIX: A mosaic Asian anthropogenic emission inventory for the MICS-Asia and the HTAP projects. *Atmospheric Chemistry and Physics*, 15(23), 34,813–34,869. <https://doi.org/10.5194/acpd-15-34813-2015>
- Li, S., Garay, M. J., Chen, L., Rees, E., & Liu, Y. (2013). Comparison of GEOS-Chem aerosol optical depth with AERONET and MISR data over the contiguous United States. *Journal of Geophysical Research: Atmospheres*, 118, 11,228–11,241. <https://doi.org/10.1002/jgrd.50867>
- Li, S., Yu, C., Chen, L., Tao, J., Letu, H., Ge, W., et al. (2016). Inter-comparison of model-simulated and satellite-retrieved componential aerosol optical depths in China. *Atmospheric Environment*, 141, 320–332. <https://doi.org/10.1016/j.atmosenv.2016.06.075>
- Liu, Y., Koutrakis, P., & Kahn, R. (2007). Estimating fine particulate matter component concentrations and size distributions using satellite-retrieved fractional aerosol optical depth: Part 1—Method development. *Journal of the Air & Waste Management Association*, 57(11), 1351–1359. <https://doi.org/10.3155/1047-3289.57.11.1351>
- Martin, R. V., Jacob, D. J., & Yantosca, R. M. (2003). Global and regional decreases in tropospheric oxidants from photochemical effects of aerosols. *Journal of Geophysical Research*, 108(D3), 4097. <https://doi.org/10.1029/2002JD002622>
- Mishchenko, M. I., Dlugach, J. M., Yanovitskij, E. G., & Zakharova, N. T. (1999). Bidirectional reflectance of flat, optically thick particulate layers: An efficient radiative transfer solution and applications to snow and soil surfaces. *Journal of Quantitative Spectroscopy and Radiation Transfer*, 63(2-6), 409–432. [https://doi.org/10.1016/S0022-4073\(99\)00028-X](https://doi.org/10.1016/S0022-4073(99)00028-X)
- Misra, A., Gaur, A., Bhattu, D., Ghosh, S., Dwivedi, A. K., Dalai, R., et al. (2014). An overview of the physico-chemical characteristics of dust at Kanpur in the central Indo-Gangetic basin. *Atmospheric Environment*, 97, 386–396. <https://doi.org/10.1016/j.atmosenv.2014.08.043>
- Misra, A., Kanawade, V. P., & Tripathi, S. N. (2016). Quantitative assessment of AOD from 17 CMIP5 models based on satellite-derived AOD over India. *Annales de Geophysique*, 34(8), 657–671. <https://doi.org/10.5194/angeo-34-657-2016>
- Murray, L. T., Jacob, D. J., Logan, J. A., Hudman, R. C., & Koshak, W. J. (2012). Optimized regional and interannual variability of lightning in a global chemical transport model constrained by LIS/OTD satellite data. *Journal of Geophysical Research*, 117, D20307. <https://doi.org/10.1029/2012JD017934>
- Ohara, T., Akimoto, H., Kurokawa, J., Horii, N., Yamaji, K., Yan, X., & Hayasaka, T. (2007). An Asian emission inventory of anthropogenic emission sources for the period 1980–2020. *Atmospheric Chemistry and Physics*, 7(16), 4419–4444. <https://doi.org/10.5194/acp-7-4419-2007>
- O'Neill, N. T., Eck, T. F., Smirnov, A., Holben, B. N., & Thulasiraman, S. (2003). Spectral discrimination of coarse and fine mode optical depth. *Journal of Geophysical Research*, 108(D17), 4559. <https://doi.org/10.1029/2002JD002975>
- Pandey, A., Sadavarte, P., Rao, A. B., & Venkataraman, C. (2014). Trends in multi-pollutant emissions from a technology-linked inventory for India: II. Residential, agricultural and informal industry sectors. *Atmospheric Environment*, 99, 341–352. <https://doi.org/10.1016/j.atmosenv.2014.09.080>
- Philip, S., Martin, R. V., Snider, G., Weagle, C. L., van Donkelaar, A., Brauer, M., et al. (2017). Anthropogenic fugitive, combustion and industrial dust is a significant, underrepresented fine particulate matter source in global atmospheric models. *Environmental Research Letters*, 12(4). <https://doi.org/10.1088/1748-9326/aa65a4>
- Prasad, A. K., & Singh, R. P. (2007). Comparison of MISR-MODIS aerosol optical depth over the Indo-Gangetic basin during the winter and summer seasons (2000–2005). *Remote Sensing of Environment*, 107(1-2), 109–119. <https://doi.org/10.1016/j.rse.2006.09.026>
- Prospero, J. M., Ginoux, P., Torres, O., Nicholson, S. E., & Gill, T. E. (2002). Environmental characterization of global sources of atmospheric soil dust identified with the Nimbus 7 Total Ozone Mapping Spectrometer (TOMS) absorbing aerosol product. *Reviews of Geophysics*, 40(1), 1002. <https://doi.org/10.1029/2000RG000095>
- Ramachandran, S., & Kedia, S. (2013). Aerosol optical properties over South Asia from ground-based observations and remote sensing: A review. *Climate*, 1(3), 84–119. <https://doi.org/10.3390/cli1030084>
- Ramanathan, V., Chung, C., Kim, D., Bettge, T., Bujia, L., Kiehl, J. T., et al. (2005). Atmospheric brown clouds: Impacts on South Asian climate and hydrological cycle. *Proceedings of the National Academy of Sciences of the United States of America*, 102(15), 5326–5333. <https://doi.org/10.1073/pnas.0500656102>
- Sadavarte, P., & Venkataraman, C. (2014). Trends in multi-pollutant emissions from a technology-linked inventory for India: I. Industry and transport sectors. *Atmospheric Environment*, 99, 353–364. <https://doi.org/10.1016/j.atmosenv.2014.09.081>
- Sanap, S. D., Ayantika, D. C., Pandithurai, G., & Niranjana, K. (2014). Assessment of the aerosol distribution over Indian subcontinent in CMIP5 models. *Atmospheric Environment*, 87, 123–137. <https://doi.org/10.1016/j.atmosenv.2014.01.017>
- Sharma, A. R., Kharol, S. K., Badarinath, K. V. S., & Singh, D. (2010). Impact of agriculture crop residue burning on atmospheric aerosol loading—A study over Punjab State, India. *Annales de Geophysique*, 28(2), 367–379. <https://doi.org/10.5194/angeo-28-367-2010>
- Sijikumar, S., Aneesh, S., & Rajeev, K. (2016). Multi-year model simulations of mineral dust distribution and transport over the Indian subcontinent during summer monsoon seasons. *Meteorology and Atmospheric Physics*, 128(4), 453–464. <https://doi.org/10.1007/s00703-015-0422-0>
- Singh, A., Rastogi, N., Patel, A., & Singh, D. (2016). Seasonality in size-segregated ionic composition of ambient particulate pollutants over the Indo-Gangetic Plain: Source apportionment using PMF. *Environmental Pollution*, 219, 906–915. <https://doi.org/10.1016/j.envpol.2016.09.010>
- Smirnov, A., Holben, B. N., Eck, T. F., Slutsker, I., Chatenet, B., & Pinker, R. T. (2002). Diurnal variability of aerosol optical depth observed at AERONET (Aerosol Robotic Network) sites. *Geophysical Research Letters*, 29(23), 2115. <https://doi.org/10.1029/2002GL016305>
- Srivastava, A. K., Tripathi, S. N., Dey, S., Kanawade, V. P., & Tiwari, S. (2012). Inferring aerosol types over the Indo-Gangetic Basin from ground based sunphotometer measurements. *Atmospheric Research*, 109–110, 64–75. <https://doi.org/10.1016/j.atmosres.2012.02.010>
- Tegen, I., & Lacis, A. A. (1996). Modeling of particle size distribution and its influence on the radiative properties of mineral dust aerosol. *Journal of Geophysical Research*, 101(D14), 19,237–19,244. <https://doi.org/10.1029/95JD03610>
- Tripathi, S. N., Dey, S., Chandel, A., Srivastava, S., Singh, R. P., & Holben, B. N. (2005). Comparison of MODIS and AERONET derived aerosol optical depth over the Ganga Basin, India. *Annales de Geophysique*, 23(4), 1093–1101. <https://doi.org/10.5194/angeo-23-1093-2005>
- Tripathi, S. N., Tare, V., Chinnam, N., Srivastava, A. K., Dey, S., Agarwal, A., et al. (2006). Measurements of atmospheric parameters during Indian Space Research Organization Geosphere Biosphere Programme Land Campaign II at a typical location in the Ganga basin: 1. Physical and optical properties. *Journal of Geophysical Research*, 111, 23209. <https://doi.org/10.1029/2006JD007278>
- World Health Organization (2016). WHO urban ambient air pollution database.
- Zender, C. S., Bian, H., & Newman, D. (2003). Mineral Dust Entrainment and Deposition (DEAD) model: Description and 1990s dust climatology. *Journal of Geophysical Research*, 108(D14), 4416. <https://doi.org/10.1029/2002JD002775>